Int. J. Environ. Sci. Technol. (2016) 13:1497–1504
DOI 10.1007/s13762-016-0987-2

ORIGINAL PAPER

Comparison of different phases of bismuth silicate nanofibers for photodegradation of organic dyes

S. S. Batool[1,2] · S. Hassan[3] · Z. Imran[2] · K. Rasool[2] · M. Ahmad[2] · M. A. Rafiq[1]

Received: 27 July 2015 / Revised: 11 February 2016 / Accepted: 2 April 2016 / Published online: 18 April 2016

Abstract Two different phases of bismuth silicate nanofibers [Bi_2SiO_5 and $Bi_4(SiO_4)_3$] were synthesized using electrospinning technique. BS nanofibers were tested for the photocatalytic degradation of methyl orange and safranin O dyes. Different phases of BS affect the photodegradation efficiency of nanofibers. Impressive enhancement in photocatalytic efficiency and BET surface area of $Bi_4(SiO_4)_3$ was observed over Bi_2SiO_5. A speedy reduction in dyes concentration was attributed to the rapid formation of oxygenated radicals by the capture of electrons and holes, generated in the BS nanofiber by UV irradiation. Therefore, the photocatalytic mechanism was elucidated using impedance spectroscopy at room temperature. The lower impedance value of $Bi_4(SiO_4)_3$ nanofibers had improved high-efficiency charge transfer capability. The cycling efficiency (30 times) and recovery characteristics pointed out that $Bi_4(SiO_4)_3$ nanofibers photocatalysts had high constancy, resilience, and regeneration ability.

Keywords $Bi_4(SiO_4)_3$ nanofibers · Crystal phases · Electrospinning · Photocatalytic activity

✉ S. S. Batool
sitwatnaqvi@comsats.edu.pk

[1] Micro and Nano Devices Group, Department of Metallurgy and Materials Engineering, Pakistan Institute of Engineering and Applied Sciences (PIEAS), P. O. Nilore, 4650 Islamabad, Pakistan

[2] Department of Physics, COMSATS Institute of Information Technology, Park Road, Chak Shahzad, 44000 Islamabad, Pakistan

[3] Centre for Climate Research and Development (CCRD), COMSATS Institute of Information Technology, Park Road, Chak Shahzad, 44000 Islamabad, Pakistan

Introduction

Water sanitation from hazardous compounds is considered as the most important research in Photocatalysis technique (Tassalit et al. 2011; Xie et al. 2016). These days, many heterogeneous semiconductor photocatalysts are being focused due to their low electron–hole pair recombination rate (Lang et al. 2014). In all these materials, bismuth-modified photocatalysts have gained remarkable attention for its promising photocatalytic applications (Bagwasi et al. 2013; Liu et al. 2015a, b). The reduction in size of the photocatalyst to nanoscale reduced the probability of recombination of photogenerated electron hole pairs (You et al. 2016). This may be due to rapid influx of carriers to the active sites on the surface. Therefore, numerous studies have been dedicated to semiconductor nanocrystals as photocatalyst (Ghoreishian et al. 2016; Lv et al. 2016). Unfortunately, spherical nanocrystals can easily agglomerate. Therefore, these types of nanocrystals have low photocatalytic efficiency. On the basis of these realities, one-dimensional semiconductor oxide nanostructures, e.g., nanofibers are superior contestants for photocatalytic application (Jung et al. 2015; Yasin et al. 2015; Yousef et al. 2016).

Photocatalysis of semiconductors is significantly influenced by their surface nature (Mao et al. 2015). In order to avoid electron hole recombination, it is necessary to have photogenerated electrons and holes available on the surface of catalysts (Gomathi Devi and Kavitha 2016). Bismuth silicate (BS) material is found in different crystalline structure with different phases, e.g., Bi_2SiO_5 and $Bi_4(SiO_4)_3$. This crystalline arrangement is dependent on working conditions, mainly on calcination temperatures. The structural analysis has revealed that Bi_2SiO_5 is a metastable phase among BS materials. These meta-

stable states are considered as the temporary energy traps (Denisova et al. 2014). In some conditions, electrons trapped in these states recombine with easily available holes and does not contribute to the degradation of toxic organic compound. Some of the metastable Bi_2SiO_5 nanostructures have shown the low degradation efficiency as compared to other BS phases (Manivel et al. 2010; Zhang et al. 2011). Moreover, photodegradation efficiency is also affected by the crystallinity (Wang et al. 2014). In this paper, the effect of different phases of BS nanofibers on photodegradation of toxic organic dyes is investigated. The cyclic efficiency and recovery characteristics of these nanofibers are also discussed. All the experimental work was done at Pakistan Institute of Engineering and Applied Sciences Islamabad, Pakistan.

Materials and methods

In this study $Bi_4(SiO_4)_3$ nanofibers used for photocatalytic application were synthesized using electrospinning technique. Polyvinylpyrrolidone (PVP, $M_w = 130$k), tetraethoxysilane (TEOS), acetic acid (CH_3COOH), and ethanol (C_2H_5OH) were used as initial materials. Bismuth acetate was used for synthesis of $Bi_4(SiO_4)_3$ nanofibers. Solution 1 was prepared by 13 % PVP/ethanol and 13 % TEOS/acetic acid. For second solution, 1 g of bismuth acetate [$Bi(C_2H_3O_2)_3$] was dissolved in 1 mL of *N*,*N*-dimethylformamide (DMF) in a capped beaker. The mixture was stirred for 30 min, then solution 1 was gradually added into solution 2. After being stirred for 90 min, the final solution was loaded into a syringe. High voltage (10 kV) was applied between the tip of the needle and collector plate (Batool et al. 2013; Hussain et al. 2014). As-spun BS nanofibers were collected on an aluminum foil placed on a conducting collector plate. These nanofibers were annealed at 500 and 600 °C for 6 h in a furnace. The annealing at 500 and 600 °C yielded Bi_2SiO_5 and $Bi_4(SiO_4)_3$ nanofibers, respectively. The photocatalytic activity of BS nanofibers was investigated by measuring photodegradation of MO and SO. The structures of both dyes are shown in Fig. 1a. An experiment was done using a homemade photoreactor. High-pressure mercury lamp (250 W) of 311 mW/cm^2 was used for irradiation. The whole experiment was carried out at ambient conditions. Distance between solution and lamp was 10 cm. During the experiment, an aliquot of 3 mL solution was strained out after each 10 min. Drained sample was centrifuged and filtered using filter paper (0.5 μm). Samples for photocatalytic measurements were prepared by adding the 1.5 g of BS nanofibers to 12.5 mmol/L of MO and SO dye solutions. The pH of dye solution was regulated using 0.1 molar solution of sodium hydroxide and hydrochloric acid and was regularly monitored. The efficacy of dye removal by photocatalyst was confirmed for different pH values, dye concentration, catalyst dosage, and contact time. Absorbance of standard dye solutions for each dye concentration was determined by means of UV–visible spectroscopy at their specific wavelengths (464 nm for MO and 525 nm for SO). Working curve based on absorbance and concentration was fine fitted by the regression equation $A = 9.9C + 0.0046$ for MO and $A = 0.1215C + 0.0001$ for SO dye, where 'A' is the absorbance and 'C' is the dye concentration. A correlation coefficient was $R^2 \cong 0.999$. The color removal efficiency of all dyes is given by (Chen et al. 2012):

$$\eta\ (\%) = \frac{C_0 - C_t}{C_0} \times 100 \quad (1)$$

Here C_0 is initial dye concentration and C_t is dye concentration after time 't' min. Schematic presentation of recycling photocatalytic activity of BS nanofibers is shown in Fig. 1b.

Results and discussion

The nanofibers annealed at 600 °C are of $Bi_4(SiO_4)_3$ phase, as reported in a previous study are also presented in this manuscript for comparison (Batool et al. 2014). However, the nanofibers annealed at 500 °C have Bi_2SiO_5 phase as shown in Fig. 1c. The pattern matches with the JCPDS, card No. 075-1483. Inset in Fig. 1c shows the SEM image of Bi_2SiO_5 and $Bi_4(SiO_4)_3$ nanofibers. The Bi_2SiO_5 has an orthorhombic crystal system and strong peaks appeared at $2\theta = 11.65°$ and $2\theta = 24.05°$ which can be associated with (2 0 0) and (1 1 1) planes, respectively. If we further heat treat the nanofibers at 600 °C, the crystalline peaks related to $Bi_4(SiO_4)_3$ phase of the BS system with JCPDS Card No. 080-1596 has been observed (Batool et al. 2014). The $Bi_4(SiO_4)_3$ has cubic phase. It also has few peaks of bismuth silicon oxide that can be removed by further heating the sample at higher temperatures (Imran et al. 2014).

Figure 1d shows the N_2 adsorption–desorption isotherms of $Bi_4(SiO_4)_3$ and Bi_2SiO_5 nanofibers. In case of $Bi_4(SiO_4)_3$, a plateau is observed which indicates that this material is mainly microporous in nature. While in Bi_2SiO_5 the plateau is not clearly obtained, which represents the widening of pores. Both types of nanofibers show a type IIb isotherm (Fig. 1d) and presence of type H4 hysteresis loop which indicates the simultaneous presence of mesopores and micropores (Zhang et al. 2014). BET values of surface areas (S_{BET}) for $Bi_4(SiO_4)_3$ and Bi_2SiO_5 nanofibers are shown in Table 1. The value of S_{BET} of the Bi_2SiO_5 (237 m^2/g) is lower than that of $Bi_4(SiO_4)_3$ (495 m^2/g). The

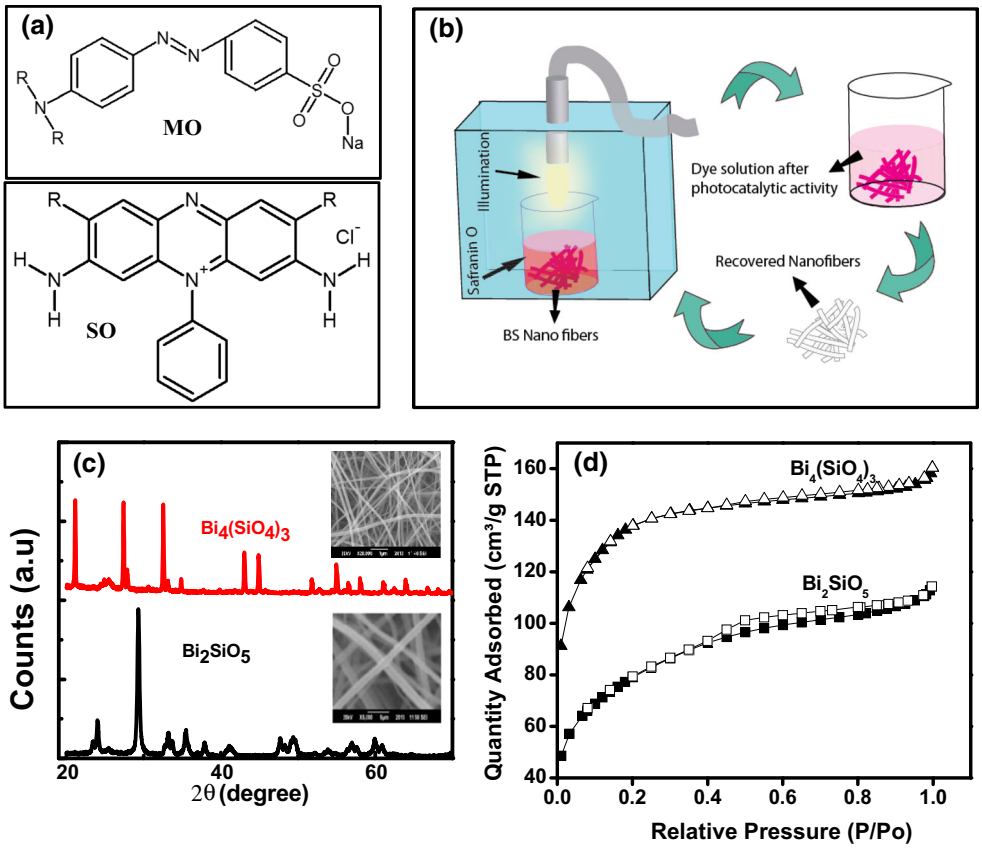

Fig. 1 **a** Structures of dyes MO and SO. **b** Schematic representation of recycling photocatalytic activity of BS nanofibers. **c** XRD pattern of Bi_2SiO_5 and $Bi_4(SiO_4)_3$ nanofibers (Hussain et al. 2014). *Inset* shows SEM image of nanofibers. **d** N_2 adsorption–desorption curve for Bi_2SiO_5 and $Bi_4(SiO_4)_3$ nanofibers

Table 1 BET N_2 adsorption analysis of BS nanofibers

Samples	BET surface area (m^2/g)	Micropore volume (t-plot) (cm^3/g)	Total pore volume (cm^3/g)
Bi_2SiO_5	237	0.025	0.18
$Bi_4(SiO_4)_3$	495	0.096	0.25

larger surface area of $Bi_4(SiO_4)_3$ attributes to the contribution of both micropores and external surface areas. The total pore volume is higher for $Bi_4(SiO_4)_3$ (0.096 cm^3/g) as compared to that of Bi_2SiO_5 (0.025 cm^3/g), respectively.

Photocatalytic efficiency of the BS system as a function of pH, intensity of light, dye concentration, and catalyst dosage for MO and SO is studied. Both phases of BS system show almost similar trends for each parameter. But $Bi_4(SiO_4)_3$ nanofibers has presented the better photodegradation efficiency as compared to Bi_2SiO_5 nanofibers catalysts. Therefore, Fig. 2 only shows the results related to $Bi_4(SiO_4)_3$ nanofibers photocatalyst. Figure 2a shows change in photodegradation efficiency of $Bi_4(SiO_4)_3$ nanofibers as pH of the solutions is varied from acidic to alkaline media (4–12). In this case, all other factors such as concentration of dye, light intensity, and photocatalyst dosage are kept constant. The photodegradation of MO is higher in acidic media (pH 4) and decreases with an increase in pH of the solution. This may be due to availability of OH^- ions in alkaline media. These ions generate a negative effect on the surface of nanofibers. As a result, the negatively charged surface repels the electron rich dye, and we get negligible photodegradation in higher pH values (Laaz et al. 2016). The photodegradation of SO is higher at neutral pH 7, but in alkaline and acidic media photocatalytic activity of BS system is low. This activity of dye elimination could be due to presence of H^+ ions in acidic media and may challenge the SO ions for the adsorption sites of BS nanofibers photocatalysts. Therefore, in this media the approach of dye molecules to the catalysts is restricted (Liu et al. 2015a, b). After acidic media, the nanofibers surface turn into negatively charged surface due to accessibility of OH^- ions. These OH^- ions produce $OH^{\cdot}$ radicals after combining with the holes of nanofibers photocatalyst. So the alkaline media up to a certain limit is considered responsible for good photocatalytic degradation efficiency (Bansal et al. 2015). In very alkaline media, it is examined that photocatalytic efficiency again decreases. This is due to maximum adsorption of dyes on the surface of photocatalyst. This may block the incident light to approach the surface of photocatalysts for further

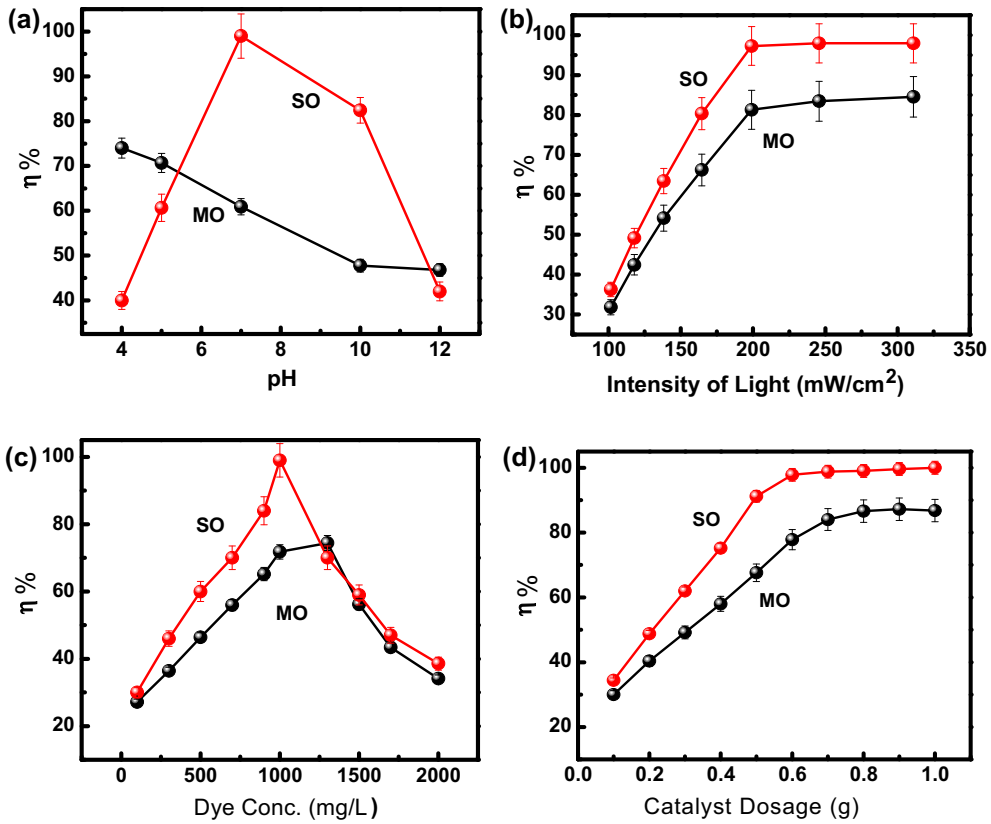

Fig. 2 Effect of **a** pH. **b** Intensity of light. **c** Dye concentration. **d** Catalyst dosage on degradation efficiency of $Bi_4(SiO_4)_3$ nanofibers

generation of electron hole pairs. Therefore, it is concluded that for SO, pH 7 is good for the photocatalytic experiment.

So as to explore the consequence of light intensity variation on photocatalytic activity of BS nanofibers, degradation of MO and SO dyes was investigated using light intensity from 101 to 311 mW/cm^2. For this purpose, 250-W mercury lamp was placed above the dye solution at 14, 13, 12, 11, 10, 9, and 8 cm. All solutions were kept in a beaker of 8 cm diameter to the core of light source. The effect of light intensity on degradation efficiency is depicted in Fig. 2b. These results tell that photodegradation rate of both dyes increases linearly with increasing the light intensity up to 311 mW/cm^2. A further increase in light intensity does not contribute to photocatalytic activity. This linear increase in degradation rate with an increase in light intensity can be clarified on the basis of excited molecules (Yu et al. 2002). As light intensity on the surface of BS nanofibers increases, availability of electron for excitation increases. Hence, additional electron hole pairs are produced on photocatalyst surface and may be available for degradation of dye molecules (Im et al. 2008).

To study the effect of dyes concentration on photocatalytic activity of BS nanofibers, the concentration of dyes varying from 10 to 200 mg/L is selected. The results are graphically shown in Fig. 2c. It can be clearly seen from the results that up to 100 mg/L, the photodegradation efficiency of BS nanofibers increases with increase in dye concentration. This may be due to accessibility of more dye molecules present in the solution (Im et al. 2008). These dye molecules cause excitation. Due to this excitation, inter-system crossing occurs, which increases the degradation efficiency. The additional amount of dye in the solution acts as a filter for the incident light intensity to reach nanofibers surface under the same condition. Therefore, the rate of photocatalytic reaction decreases (Yu et al. 2005).

Photocatalyst dosage also affects the photocatalytic efficiency of BS nanofibers. For this purpose, the amount of catalysts is varied from 0.1 to 1 g remaining all other parameters constant. The consequences are presented in Fig. 2d. We can see from the curve that increase in catalysts dosage causes an increase in photodegradation efficiency until the saturation point come. After the saturation limit, the degradation efficiency dramatically decreases with further increase in catalysts dosage. Surface area of photocatalyst is increased, when we increase the catalysts amount. Therefore, rate of photoreaction increases (Kansal et al. 2007). Even though, a further amount of catalyst in

Table 2 Comparison of photocatalytic performance of BS nanofibers with different nanocompounds for degradation of organic dyes

Catalysts	Catalyst structure	Photodegradation (%)	Time (min)	Degradation rate	References
La- and B-doped $BiVO_4$	Nanoparticles	98.4	60	0.075/min	Min et al. (2013)
$BiOCl/Bi_4Ti_3O_{12}$	Nanofibers	91	40	–	Zhang et al. (2015a, b)
0.1 g β Bi_2O_3	Nanocomposite	94.3	50	0.004/min	Iyyapushpam et al. (2015)
TiO_2/MoS_2	Nanocomposite	95	60	2.304/h	Zhang et al. (2015a, b)
Bi-modified SiO_2/Bi_2SiO_5	Powder	28	90	0.1877/h	Police et al. (2013)
$BiVO_4$	Microtubes	90	200	0.06464/min	Ying et al. (2015)
$Bi_4(SiO_3)_4$	Nanofibers	80	80	0.273/min	Present work
Bi_2SiO_5	Nanofibers	60	80	0.149/min	

solution will increase the number of active sites for photocatalytic reaction. Subsequent to saturation point, additional amount of catalyst dosage does not take part in exposed surface area for photocatalytic reaction. It will merely enhance the nanofibers concentration beneath the beaker. Due to these thick layers of flakes, light may not penetrate through the solution and resist further absorption of photons, which reduces the photodegradation rate due to light dispersion and screening (Madhu et al. 2007). The transaction between aforementioned two contrasting phenomena is an outcome of a more favorable catalyst dosage for the photocatalytic reaction. The optimum catalysts dosage for this experiment is 0.6 g.

We investigated the photodegradation efficiency of the Bi_2SiO_5 and $Bi_4(SiO_4)_3$ nanofibers for removal of MO and SO dyes. The data are shown in the Fig. 3. The pH is adjusted to 4.0 for MO suspension and 7.0 for SO suspension. Change in pH value throughout the experiment is negligibly small. The degradation of MO and SO is in the order of $Bi_2SiO_5 < Bi_4(SiO_4)_3$ under the experimental condition used. Insets of Fig. 3a, b show the digital camera photographs demonstrating the change in color with time for MO and SO, respectively. In case of Bi_2SiO_5 nanofibers photocatalyst, degradation efficiency is 60 % for MO and 70 % for SO in 120 min. But for the case of $Bi_4(SiO_4)_3$ nanofibers photocatalyst, the degradation rate increases for both dyes, 80 % for MO and 92 % for SO in the same time slot. The above results show that the photocatalytic activity of $Bi_4(SiO_4)_3$ nanofibers is perceptibly better than that of Bi_2SiO_5 nanofibers photocatalysts. Therefore, we can say that $Bi_4(SiO_4)_3$ nanofibers photocatalyst has universality for the degradation of different organic dyes. The photocatalytic reaction can also be considered as a photoelectrochemical process (Zhang et al. 2013). The results can be proved by impedance spectroscopy of the same material (inset of Fig. 3c). The radius of the arc on the Cole–Cole plot of the $Bi_4(SiO_4)_3$ nanofibers is smaller than that of Bi_2SiO_5 nanofibers. This means that the former has improved high-efficiency charge transfer capability (Dong et al. 2014). This phenomenon favors detain of H_2O_2 molecules to capitulate hydroxyl radicals (˙OH) for decaying toxic dyes (Huang et al. 2013). Furthermore, the result is also supported by the large surface area of $Bi_4(SiO_4)_3$ nanofibers (495 m^2/g) as compared to Bi_2SiO_5 nanofibers (237 m^2/g). Large surface area of photocatalysts also plays an important role in enhancing the photodegradation efficiency (Kim et al. 2014).

The degradation rate of MO and SO dye aqueous solutions is examined using pseudo-first-order kinetic reaction. Thus, the following equation is used to discuss their kinetics:

$$\ln(C_0/C_t) = k_{app}t \quad (2)$$

where C_0 is a concentration of dye prior to photodegradation (mg/L), C_t is the dye concentration at reaction time t for decolourization, and k_{app} is the apparent rate constant (min^{-1}) (Batool et al. 2014). The apparent rate constant k_{app} of the Bi_2SiO_5 nanofibers and $Bi_4(SiO_4)_3$ nanofibers for MO and SO dyes is found by fitting the experimental data (Fig. 3a, b). It can be realized that the values of k_{app} of the $Bi_4(SiO_4)_3$ nanofibers for degradation of MO and the SO are 0.273 (min^{-1}) and 0.409 (min^{-1}), respectively. In the case of Bi_2SiO_5 nanofibers, the degradation rate is 0.149 (min^{-1}) and 0.301 (min^{-1}), respectively. On the basis of our results, we describe the mechanism of photocatalytic activity of BS nanofibers.

Electron–hole pair is generated in BS nanofibers under UV irradiation. These photogenerated electrons may react with the absorbed O_2 molecules from its surroundings to form reactive O_2^-. This may suggested that the recombination is slowed and the generation of O_2^- species is accelerated. These O_2^- radicals are the main cause of enhanced activity of BS nanofibers. The reaction can be presented as follows:

$$BS + h\upsilon \rightarrow BS + h^+_{\upsilon B} + e^-_{cB}$$

Electron entrapping

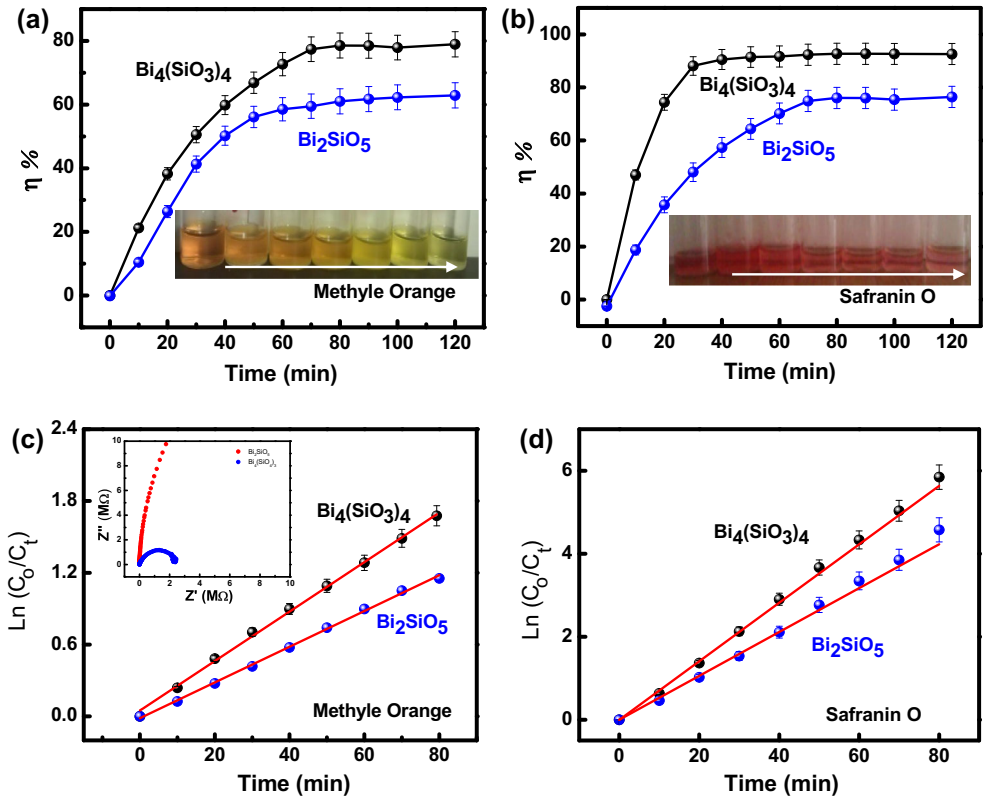

Fig. 3 Photodegradation of **a** MO and **b** SO by Bi_2SiO_5 and $Bi_4(SiO_4)_3$ nanofibers at 273 K with initial dye concentration 12.5 mmol/L. *Insets* show the digital camera photographs demonstrating the change in color with time for respective dyes. Kinetic study of **c** MO and **d** SO. *Inset* to **c** shows the Cole–Cole plot of Bi_2SiO_5 and $Bi_4(SiO_4)_3$ nanofibers at room temperature

$$O_2 + e_{cB}^- \rightarrow O_2^-$$

Radical generation

$$H^+ + H_2O \rightarrow H^+ + HO^{\cdot}$$

Product formation

$$HO^{\cdot} + \text{MO/SO dyes} \rightarrow \text{degradation of dye molecules}$$

These radicals are moved into the molecular structure of dyes (Zhang et al. 2011). The conjugated system of dyes are dislocated and causes the complete decomposition of MO and SO in case of $Bi_4(SiO_4)_3$ nanofibers photocatalyst. But in case of Bi_2SiO_5 nanofibers photocatalyst, small surface area may affect the complete decomposition of dyes. These radicals may be the reasons for the oxidation of other organic compounds (Ullah and Dutta 2008; Mohamed et al. 2016).

Moreover, the cycle procedure of the photodegradation of MO and the SO is carried out to check the stability and regeneration capability of photocatalysts. Results are depicted in Fig. 4. The photocatalytic efficiency of $Bi_4(SiO_4)_3$ nanofibers is not apparently lost within 30 cycles. Reaction time for this experiment was 3600 min. But after 30th cycle the removal efficiency started to decrease. After the 30th cycle, color of samples changes from white to dark yellow (MO) and shocking pink (SO). We then washed the samples using de-ionized water to remove the adsorbed dyes after drying the sample for 24 h. The original color of the samples is retrieved upon undergoing re-calcinations process after 10 washes. The photodegradation efficiency of regenerated samples up to ten cycles is shown in Fig. 4c. It is clear from the graph that the degradation efficiency is almost same as that of fresh sample. It specifies that $Bi_4(SiO_4)_3$ nanofibers photocatalyst holds remarkable stability, durability, and regeneration capability. Comparison of photocatalytic performance of BS nanofibers with different nanocompounds for degradation of organic dyes are shown in Table 2.

Conclusion

In summary, we reported the effect of different phases [$Bi_4(SiO_4)_3$ and Bi_2SiO_5 nanofibers] of BS system on photodegradation of cationic and anionic dyes. It was confirmed that $Bi_4(SiO_4)_3$ had improved high-efficiency

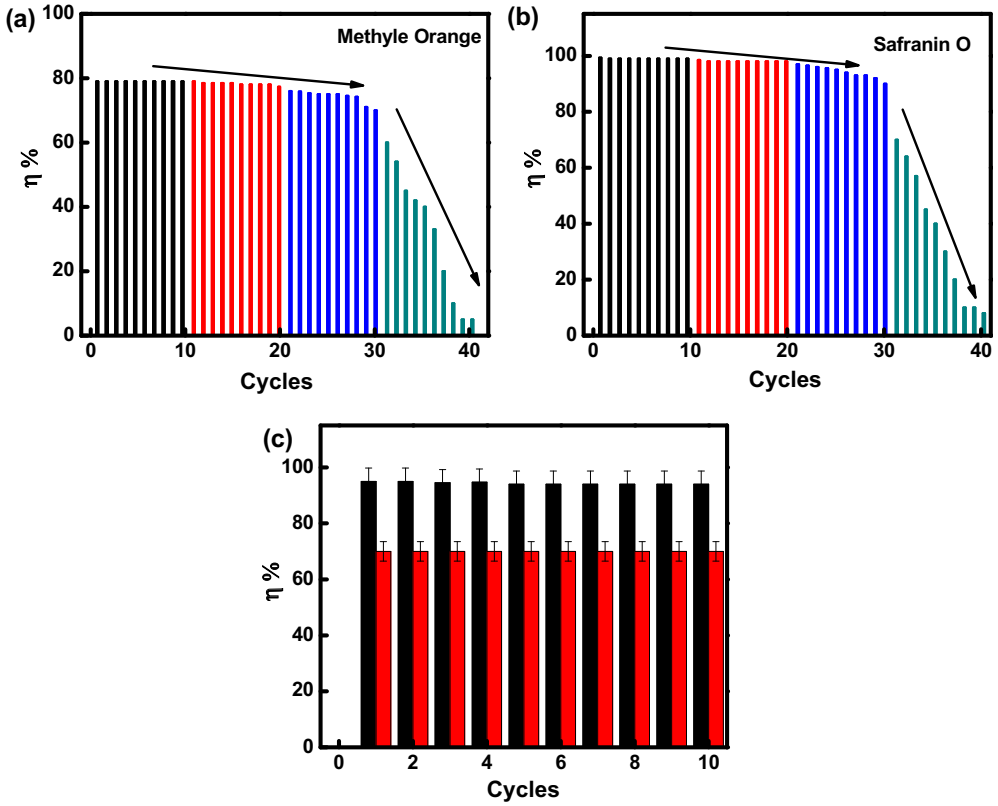

Fig. 4 Cycle procedure of the **a** MO and **b** SO of $Bi_4(SiO_4)_3$ nanofibers. **c** Cycle procedure performed on $Bi_4(SiO_4)_3$ nanofibers after regeneration of catalysts

charge transfer capability than that of Bi_2SiO_5 nanofibers. Furthermore, kinetic results was best fitted by the pseudo-first-order model revealed that $Bi_4(SiO_4)_3$ nanofibers had a high degradation rate of 0.273 and 0.409 (min^{-1}) for MO and SO, respectively. $Bi_4(SiO_4)_3$ nanofibers proved to be an effective photocatalyst.

Acknowledgments The authors would like to acknowledge higher education commission Pakistan for their financial support under Indigenous Ph.D. 5000 Fellowship Program Phase-IV with Grant No. 17-5-4(Ps4-504) HEC/Sch/2007/.

References

Bagwasi S, Niu Y, Nasir M, Tian B, Zhang J (2013) The study of visible light active bismuth modified nitrogen doped titanium dioxide photocatalysts: role of bismuth. Appl Surf Sci 264:139–147

Bansal P, Chaudhary GR, Mehta SK (2015) Comparative study of catalytic activity of ZrO_2 nanoparticles for sonocatalytic and photocatalytic degradation of cationic and anionic dyes. Chem Eng J 280:475–485. doi:10.1016/j.cej.2015.06.039

Batool S, Imran Z, Israr M, Usman M, Jamil H, Rafiq M, Hassan M, Willander M (2013) Comparative analysis of Ti, Ni, and Au electrodes on characteristics of TiO_2 nanofibers for humidity sensor application. J Mater Sci Technol 29:411–414

Batool S, Hassan S, Imran Z, Rafiq M, Ahmad M, Rasool K, Chaudhry M, Hasan M (2014) The enhancement in photocatalytic activity of bismuth modified silica and bismuth silicate nanofibers. Catal Commun 49:39–42

Chen Y, Li D, He M, Hu Y, Ruan H, Lin Y, Hu J, Zheng Y, Shao Y (2012) High photocatalytic performance of zinc hydroxystannate toward benzene and methyl orange. Appl Catal B Environ 113:134–140

Denisova L, Irtyugo L, Denisov V (2014) Heat capacity of oxides in the Bi_2O_3–SiO_2 system. Phys Solid State 56(10):2146–2148

Dong H, Chen G, Sun J, Feng Y, Li C, Lv C (2014) Stability, durability and regeneration ability of a novel Ag-based photocatalyst, Ag_2 Nb_4 O_{11}. Chem Commun 50(50):6596–6599

Ghoreishian SM, Badii K, Norouzi M, Malek K (2016) Effect of cold plasma pre-treatment on photocatalytic activity of 3d fabric loaded with nano-photocatalysts: response surface methodology. Appl Surf Sci 365:252–262. doi:10.1016/j.apsusc.2015.12.155

Gomathi Devi L, Kavitha R (2016) A review on plasmonic metal–TiO_2 composite for generation, trapping, storing and dynamic vectorial transfer of photogenerated electrons across the Schottky junction in a photocatalytic system. Appl Surf Sci 360(Part B):601–622. doi:10.1016/j.apsusc.2015.11.016

Huang Q, Tian S, Zeng D, Wang X, Song W, Li Y, Xiao W, Xie C (2013) Enhanced photocatalytic activity of chemically bonded TiO2/graphene composites based on the effective interfacial charge transfer through the C-Ti bond. ACS Catal 3(7):1477–1485

Hussain M, Batool SS, Imran Z, Ahmad M, Rasool K, Rafiq M, Hasan M (2014) Oxygen sensing and transport properties of nanofibers of silica, bismuth doped silica and bismuth silicate prepared via electrospinning. Sens Actuators B Chem 192:429–438

Im JS, Kim MI, Lee Y-S (2008) Preparation of pan-based electrospun nanofiber webs containing TiO_2 for photocatalytic degradation. Mater Lett 62(21):3652–3655

Imran Z, Batool SS, Rafiq MA, Rasool K, Ahmad M, Shahid R, Hasan M (2014) Investigation of change in surface area and grain size of cadmium titanate nanofibers upon annealing and their effect on oxygen sensing. ACS Appl Mater Interface 6(6):4542–4549

Iyyapushpam S, Nishanthi S, Padiyan DP (2015) Synthesis of β-Bi_2O_3 towards the application of photocatalytic degradation of methyl orange and its instability. J Phys Chem Solids 81:74–78

Jung J-Y, Lee D, Lee Y-S (2015) Cnt-embedded hollow TiO_2 nanofibers with high adsorption and photocatalytic activity under UV irradiation. J Alloys Compd 622:651–656. doi:10.1016/j.jallcom.2014.09.068

Kansal S, Singh M, Sud D (2007) Studies on photodegradation of two commercial dyes in aqueous phase using different photocatalysts. J Hazard Mater 141(3):581–590

Kim WJ, Pradhan D, Min B-K, Sohn Y (2014) Adsorption/photocatalytic activity and fundamental natures of BiOCl and $BiOCl_xI_{1-x}$ prepared in water and ethylene glycol environments, and Ag and Au-doping effects. Appl Catal B Environ 147:711–725

Laaz I, Stébé M-J, Benhamou A, Zoubir D, Blin J-L (2016) Influence of porosity and surface modification on the adsorption of both cationic and anionic dyes. Colloid Surf A Physicochem Eng Asp 490:30–40. doi:10.1016/j.colsurfa.2015.11.024

Lang X, Chen X, Zhao J (2014) Heterogeneous visible light photocatalysis for selective organic transformations. Chem Soc Rev 43(1):473–486

Liu Y, Zeng G, Tang L, Cai Y, Pang Y, Zhang Y, Yang G, Zhou Y, He X, He Y (2015a) Highly effective adsorption of cationic and anionic dyes on magnetic Fe/Ni nanoparticles doped bimodal mesoporous carbon. J Colloid Interface Sci 448:451–459. doi:10.1016/j.jcis.2015.02.037

Liu Z, Lu Q, Wang C, Liu J, Liu G (2015b) Preparation of bamboo-shaped BiVO4 nanofibers by electrospinning method and the enhanced visible-light photocatalytic activity. J. Alloy. Comp. 651:29–33. doi:10.1016/j.jallcom.2015.08.125

Lv X-J, Zhou S, Huang X, Wang C, Fu W-F (2016) Photocatalytic overall water splitting promoted by SnO_x–$NiGa_2O_4$ photocatalysts. Appl Catal B Environ 182:220–228. doi:10.1016/j.apcatb.2015.09.032

Madhu G, Raj M, Pai KVK, Rao S (2007) Photodegradation of methylene blue dye using UV/$BaTiO_3$, UV/H_2O_2 and UV/H_2O_2/$BaTiO_3$ oxidation processes. Ind J Chem Technol 14(2):139–144

Manivel A, Naveenraj S, Kumar S, Selvam P, Anandan S (2010) CuO-TiO_2 nanocatalyst for photodegradation of acid red 88 in aqueous solution. Sci Adv Mater 2(1):51–57

Mao X, Wang Z, Lang X, Hao Q, Wen B, Dai D, Zhou C, Liu L-M, Yang X (2015) Effect of surface structure on the photoreactivity of TiO_2. J Phys Chem C 119(11):6121–6127

Min W, Yinsheng C, Chao N, Mingyan D, Duo D (2013) Lanthanum and boron Co-doped $BiVO_4$ with enhanced visible light photocatalytic activity for degradation of methyl orange. J Rare Earth 31(9):878–884

Mohamed A, El-Sayed R, Osman TA, Toprak MS, Muhammed M, Uheida A (2016) Composite nanofibers for highly efficient photocatalytic degradation of organic dyes from contaminated water. Environ Res 145:18–25. doi:10.1016/j.envres.2015.09.024

Police AKR, Basavaraju S, Valluri DK, Machiraju S (2013) Bismuth modified porous silica preparation, characterization and photocatalytic activity evaluation for degradation of isoproturon. J Mater Sci Technol 29(7):639–646

Tassalit D, Laoufi A, Bentahar F (2011) Photocatalytic deterioration of tylosin in an aqueous suspension using UV/TiO_2. Sci Adv Mater 3(6):944–948

Ullah R, Dutta J (2008) Photocatalytic degradation of organic dyes with manganese-doped ZnO nanoparticles. J Hazard Mater 156(1):194–200

Wang X, Sø L, Su R, Wendt S, Hald P, Mamakhel A, Yang C, Huang Y, Iversen BB, Besenbacher F (2014) The influence of crystallite size and crystallinity of anatase nanoparticles on the photodegradation of phenol. J Catal 310:100–108. doi:10.1016/j.jcat.2013.04.022

Xie M, Wei W, Jiang Z, Xu Y, Xie J (2016) Carbon nitride nanowires/nanofibers: a novel template-free synthesis from a cyanuric chloride–melamine precursor towards enhanced adsorption and visible-light photocatalytic performance. Ceram Int 42(3):4158–4170. doi:10.1016/j.ceramint.2015.11.089

Yasin AS, Obaid M, El-Newehy MH, Al-Deyab SS, Barakat NAM (2015) Influence of $Ti_xZr_{(1-x)}O_2$ nanofibers composition on the photocatalytic activity toward organic pollutants degradation and water splitting. Ceram Int 41(9, Part B):11876–11885. doi:10.1016/j.ceramint.2015.05.156

Ying Y, Tao F, Hong T, Wang L (2015) Controlled fabrication of bismuth vanadium oxide hierarchical microtubes with enhanced visible light photocatalytic activity. Mater Sci Semiconduct Process 32:82–89. doi:10.1016/j.mssp.2015.01.009

You D, Pan B, Jiang F, Zhou Y, Su W (2016) Cds nanoparticles/CeO_2 nanorods composite with high-efficiency visible-light-driven photocatalytic activity. Appl Surf Sci 363:154–160. doi:10.1016/j.apsusc.2015.12.021

Yousef A, Brooks RM, El-Halwany MM, El-Newehy MH, Al-Deyab SS, Barakat NAM (2016) CuO/s-doped TiO_2 nanoparticles-decorated carbon nanofibers as novel and efficient photocatalyst for hydrogen generation from ammonia borane. Ceram Int 42(1, Part B):1507–1512. doi:10.1016/j.ceramint.2015.09.097

Yu JC, Yu J, Ho W, Jiang Z, Zhang L (2002) Effects of F-doping on the photocatalytic activity and microstructures of nanocrystalline TiO_2 powders. Chem Mater 14(9):3808–3816

Yu Y, Yu JC, Chan C-Y, Che Y-K, Zhao J-C, Ding L, Ge W-K, Wong P-K (2005) Enhancement of adsorption and photocatalytic activity of TiO_2 by using carbon nanotubes for the treatment of azo dye. Appl Catal B Environ 61(1):1–11

Zhang P, Hu J, Li J (2011) Controllable morphology and photocatalytic performance of bismuth silicate nanobelts/nanosheets. RSC Adv 1(6):1072–1077

Zhang Z, Dua R, Zhang L, Zhu H, Zhang H, Wang P (2013) Carbon-layer-protected cuprous oxide nanowire arrays for efficient water reduction. ACS Nano 7(2):1709–1717

Zhang J, He D, Su H, Chen X, Pan M, Mu S (2014) Porous polyaniline-derived fen x c/c catalysts with high activity and stability towards oxygen reduction reaction using ferric chloride both as an oxidant and iron source. J Mater Chem A 2(5):1242–1246

Zhang M, Liu Y, Li L, Gao H, Zhang X (2015a) Biocl nanosheet/$Bi_4Ti_3O_{12}$ nanofiber heterostructures with enhanced photocatalytic activity. Catal Commun 58:122–126. doi:10.1016/j.catcom.2014.09.021

Zhang W, Xiao X, Zheng L, Wan C (2015b) Fabrication of TiO_2/MoS_2@ zeolite photocatalyst and its photocatalytic activity for degradation of methyl orange under visible light. Appl Surf Sci 358:468–478